MDPI

Review

High-Entropy Alloy Films

Kaixuan Cui and Yong Zhang * iD

State Key Laboratory for Advanced Metals and Materials, University of Science and Technology Beijing, Beijing 100083, China
* Correspondence: drzhangy@ustb.edu.cn

Abstract: High-entropy alloy films have the same excellent properties as high-entropy alloys and can better realize the practical applications of high-entropy alloys. This paper takes the high-entropy alloy films as the object of discussion. The preparation process, microstructure, hardness, wear resistance and corrosion resistance of high-entropy alloy films are mainly discussed and the influence of nitridation, sputtering power, substrate temperature, substrate bias and other factors on the phase structure of alloy films is analyzed. High-entropy alloy films can be prepared using magnetron sputtering, laser cladding, pulsed laser deposition, detonation spraying, electrochemical deposition and other processes. High-entropy alloy films tend to form a solid solution and amorphous state, and their hardness is far higher than that of traditional films. Among them, the hardness of high-entropy alloy nitride films can reach the standard of superhard films. Wear resistance is usually proportional to hardness. Due to the corrosion-resistant elements and amorphous structure, some high-entropy alloy films have better corrosion resistance than stainless steel. High-entropy alloy films have shown profound development prospects in the fields of wear-resistant coatings for tools, corrosion protection, diffusion barrier and photothermal conversion coatings.

Keywords: high-entropy alloy films; preparation process; hardness; wear resistance; corrosion resistance

1. Introduction

Traditional alloys are based on one or two elements as the main components, while adding small amounts of other elements to improve its properties, such as copper and titanium alloys. According to the traditional design concept, as long as there are too many elements in the alloys, no matter metal or non-metal, a large number of brittle intermetallic compounds will be precipitated, which greatly affects the mechanical properties of the alloys. The traditional alloy design concept has certain limitations. With this limitation, the concept of high-entropy alloys (HEAs) was proposed by Jien-Wei Yeh [1] and Cantor [2]. Compared with traditional alloys, HEAs have some excellent properties. Refractory high-entropy alloys have a high compressive yield strength at room temperature, excellent high-temperature properties, high-temperature softening resistance and wear resistance [3]. Light-weight high-entropy alloys generally have high strength, high hardness, excellent high-temperature oxidation resistance and corrosion resistance [4]. Cantor alloys have excellent cryogenic properties [5]. Eutectic high-entropy alloys have high strength and ductility at room temperature [6]. However, replacing all existing critical components with high-entropy alloys is not in line with the actual cost efficiency and it is difficult to push them to scale production. High-entropy alloy films (HEAFs) can be defined as multiple-component films with high-entropy mixing [7]. HEAFs not only exhibit excellent properties similar to those of the high-entropy alloy bulk material, but also are superior to the alloy bulk material in some properties, such as high hardness, elastic modulus and corrosion resistance. Liao et al. [8] reported that the hardness of $CoCrFeNiAl_{0.3}$ high-entropy alloy thin film is about four times that of the same-composition bulk alloy.

The research on HEAFs can be traced back to 2004. Chen et al. [9] successfully prepared FeCoNiCrCuAlMn and $FeCoNiCrCuAl_{0.5}$ high-entropy alloy films and nitriding

films using direct current magnetron sputtering technology. After that, the research on high-entropy alloy films has become more and more extensive. Considering that high-entropy alloys are mainly applied to improve the surface properties of materials, this paper takes high-entropy alloy films as the object of discussion and summarizes the preparation process, crystal structure and properties of HEAFs.

2. Methods

Various process methods have been developed to prepare HEAFs, which can be classified as magnetron sputtering, laser cladding, pulsed laser deposition, explosion spraying and electrochemical deposition.

2.1. Magnetron Sputtering

Magnetron sputtering is the most commonly used method for the preparation of HEAFs. As shown in Figure 1, the principle of magnetron sputtering is that under the action of electric and magnetic fields, Ar atoms ionize to produce Ar^+ and electrons and bombard the cathode target with high energy, so that the metal on the surface of the target is sputtered out in the form of atomic state or ionic state and finally deposited on the substrate. The preparation of HEAFs using magnetron sputtering technology has the advantages of fast deposition speed, low substrate temperature, high film quality and stable process. Thus, sputtering technology is a good method for preparing multiprincipal solid solution films [10]. According to the current mode, magnetron sputtering can be divided into direct current (DC) magnetron sputtering and radio frequency (RF) magnetron sputtering. DC magnetron sputtering is suitable for conductive targets. If insulator targets are used, it will cause "target poisoning". During the sputtering process, the target surface is oxidized, resulting in a significant reduction in the target's conductivity and the sputtering rate, which also tends to cause "target poisoning". RF magnetron sputtering is applicable to any target.
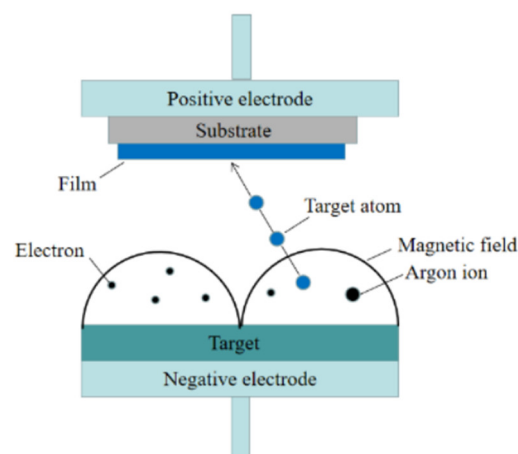
Figure 1. Schematic diagram of magnetron sputtering method.

Depending on the number of targets, magnetron sputtering deposition methods can be divided into single-target sputtering and multi-target sputtering. Sputtering targets are generally obtained with bulk high-entropy alloys preparation methods (arc melting method, powder metallurgy method, etc.). If the melting points of the elements in the high-entropy alloys are widely different, it is more suitable to be prepared using powder metallurgy. Khan et al. [11] employed a single-target magnetron sputtering method to prepare $AlCoCrCu_{0.5}FeNi$ high-entropy alloy film. The target material used was a high-purity bulk high-entropy alloy material with the same composition that was prepared with a vacuum arc melting method. Braeckman et al. [12] also adopted a single-target magnetron sputtering method to prepare AlCoCrCuFeNi HEAFs; the target material was

also a high-entropy alloy bulk material of the same composition. However, the target was prepared with the powder metallurgy method. In 2013, Feng et al. [13] prepared ZrNbTaTiW refractory high-entropy alloy films using magnetron sputtering with multiple targets (TiW alloy target, TaNb alloy target and Zr metal target). Multi-target sputtering makes the magnetron sputtering process more flexible and overcomes the difficulty that some multi-principal alloy targets are not easy to prepare, and by regulating the power, position and combination of each target, the content of each element in the film can be adjusted, which is beneficial to observe the effect of the change of certain element content on the microstructure and properties of the film [14].

2.2. Laser Cladding

The laser cladding method is an emerging surface-modification technology that uses a high-power and high-speed laser to melt the alloy powder and metallurgically bond it with the substrate surface, thus improving the hardness, wear resistance and corrosion resistance of the substrate surface. Compared with the thickness of the films prepared using the magnetron sputtering method, which reach the micron size, the thickness of the high-entropy films prepared with this method is higher, reaching the millimeter level, and the process is close to the solidification state of the bulk alloys, but has not yet reached the thickness of the bulk; thus, it is usually referred to as high-entropy alloy coating [15].

The first domestic and international research on the preparation of high-entropy alloy coatings with laser melting technology was reported in 2010 [16]. Zhang et al. [16] prepared $NiCoFeCrAl_3$ high-entropy alloy coating on Q235 steel substrate using laser cladding technology. The coating had an ordered BCC (body-centered cubic) and a small amount of FCC (face-centered cubic) simple solid solution structure. The microhardness of the coating was above 800 HV. Subsequently, Zhang et al. [17–20] investigated the microstructure, hardness, corrosion resistance and softening resistance of high-entropy alloy coatings prepared with laser cladding such as $FeCoNiCrAl_2Si$, 6FeNiCoSiCrAlTi, CoCrCuFeNi and $FeCoNiCrCuTiMoAlSiB_{0.5}$. So far, studies on the preparation of high-entropy alloy coatings with laser cladding technology have mainly focused on the influence of alloy elements [21,22], cladding process parameters (such as laser power [23], spot type [24] and scanning speed [25]) on the microstructure and properties of the coatings. At present, the selected substrate materials mainly include Q235, tool steel, etc. Table 1 shows the phase composition and hardness of high-entropy alloy coatings prepared using laser cladding.

Table 1. Phase composition and hardness of high-entropy alloy coating prepared with laser cladding.

Alloy	Substrate	Phase Composition	Hardness	Reference
$NiCoFeCrAl_3$ + little C/Si/Mn/Mo	Q235	BCC + FCC	800 HV	[16]
$FeCoNiCrAl_2Si$	Q235	BCC	900 $HV_{0.5}$	[17]
6FeNiCoSiCrAlTi	Q235	BCC	780 $HV_{0.5}$	[18]
FeCoNiCrCu + Si, Mn, Mo	Q235	FCC	450 HV with addition of Si, Mn, Mo	[19]
$FeCoNiCrCuTiMoAlSiB_{0.5}$	Medium-carbon-steel	BCC + B2	11.3 Gpa	[20]
$Al_2CrFeCo_xCuNiTi$	Q235	FCC + BCC_1 + BCC_2 + Laves	Up to 1013 HV	[21]
MoFeCrTiW + Si/Al	Q235	The main phase: BCC		[22]
NbMoTaTi	Pure Mo	BCC	397.6 HV	[23]
MoFeCrTiWAlNb	W6Mo5Cr4V2	Round spot, BCC + MC carbide	680 HV	[24]
		Rectangular spot, BCC + hcp-Fe_2Nb + MC carbide	850 HV	

Table 1. *Cont.*

Alloy	Substrate	Phase Composition	Hardness	Reference
$Al_xCoCrNiMo$	45# steel	x = 1, Cr + AlNi + Co_2C + $Fe_{63}Mo_{37}$	950–1250 $HV_{0.2}$	[25]
		x = 1.5, Cr + AlNi + Al_2FeCo + $Fe_{63}Mo_{37}$		
		x = 2, AlFe + CrMo		
		x = 2.5, AlFe + CrMo		
FeCrNiCoMn	45# steel	FCC + BCC	540 $HV_{0.2}$	[26]
AlFeCoCrNi	Al	BCC_1 + BCC_2		[27]
$Al_2CrFeNiCoCuTi_x$	Q235	FCC + BCC_1 + BCC_2 + Laves		[28]
AlCoCrCuFeNi	Mg	FCC + BCC		[29]
AlCoCrFeNi	Al	BCC_1 + BCC_2 + Al_3Ni + $FeAl_3$		[30]
TiVCrAlSi	Ti-6Al-4V	$(Ti, V)_5Si_3$ + BCC		[31]

2.3. Pulsed Laser Deposition

Pulsed laser deposition refers to the focused action of a high-powered pulsed laser generated by lasers on the surface of the target material, which generates a high-temperature, high-pressure plasma due to the high temperature and ablation, and then the plasma expands locally to form films by deposition on the substrate [32], as shown in Figure 2. In 2018, Cropper [33] prepared AlCrFeCoNiCu HEAFs with pulsed laser deposition. The films deposited at room temperature had a FCC and BCC dual-phase structure, and both crystal structures decreased with the increase in deposition temperature. In 2019, Lu et al. [34] prepared $CoCrFeNiAl_{0.3}$ HEAFs with some nanoscale particles present on the film surface. Compared with bulk alloys, thin-film materials have a higher nanohardness and lower elastic modulus and can be used for functional micro–nano devices.
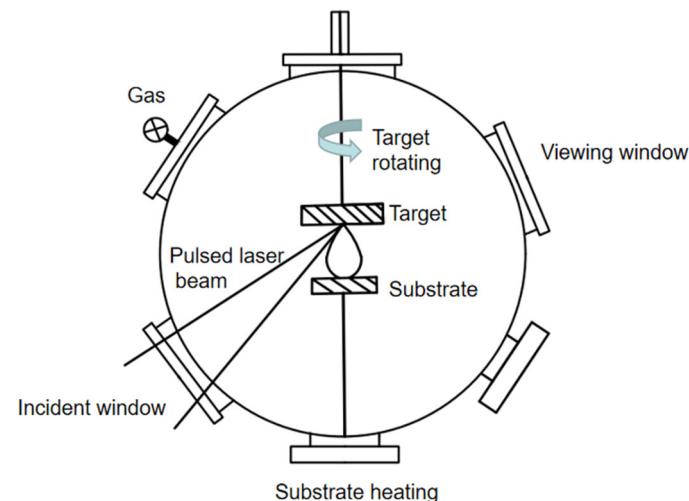

Figure 2. Schematic diagram of pulsed laser deposition.

2.4. Detonation Spraying

The conventional thermal spraying technique for preparing high-entropy alloy coatings suffers from lamellar structure, segregation and bulk oxidation. Detonation spraying technology with a short heating time can effectively suppress the segregation and oxidation of the coatings and is suitable for depositing high-quality coatings. In 2021, CoCrFeMnNi high-entropy alloy coatings were prepared for the first time with detonation spraying technology. The flocculated nano-multicomponent metal oxides were uniformly distributed

in the substrate. The microhardness of the high-entropy alloy coatings prepared with detonation spraying technology was much higher than that of casting and spark plasma sintering, which can be attributed to the nano-metal oxide enhancement and fine-grain strengthening. The CoCrFeMnNi high-entropy alloy coatings prepared using detonation spraying have good adhesion and the failure of the coatings mainly originates from laminar peeling [35].

As there are only a limited number of high-entropy alloy powder materials available in the market, the high-entropy alloy coatings are thermally sprayed using pre-alloyed powder produced with ball milling or gas atomization. Batraev et al. [36] studied the deposition of high-entropy alloy coatings using detonation spraying combined with laser cladding. Detonation spraying allows the formation of composite coatings with uniform distribution of different metal lamellae, and the coating after laser cladding forms an FCC solid solution. This method enables the preparation of high-entropy alloy coatings with any combination of metal elements.

2.5. Electrochemical Deposition

Under the action of an electric field, in a certain electrolyte solution, through an oxidation–reduction reaction, metal ions are reduced at the cathode and deposited into films, which is called electrochemical deposition. Electrochemical deposition requires no complex equipment, can be carried out at low processing temperatures and energy consumption and can be deposited on substrate surfaces with complex geometries. The main difficulty in the preparation of HEAFs using electrochemical deposition is to find a suitable electrolyte in which multiple ions can be dissolved in solution at the same time. HEAs contain a large variety of elements and the reduction potentials of different metal atoms vary greatly, making it difficult to prepare uniform high-entropy alloy films using electrochemical deposition. In 2008, Yao et al. [37] obtained Bi-Fe-Co-Ni-Mn HEAFs using potentiostatic electrodeposition in the DMF-CH_3CN system. In 2011, Yao et al. [38] prepared Nd-Fe-Co-Ni-Mn high-entropy alloy magnetic films with electrochemical deposition at room temperature. The nanostructure and surface morphology of the films can be controlled by adjusting the deposition parameters (deposition potential, deposition time).

3. Results
3.1. Phase and Microstructure

While studying bulk HEAs, scholars applied the idea of multiple high entropy to film materials and developed high-entropy alloy films. Bulk HEAs tend to form a simple disordered solid solution, while high-entropy alloy films tend to form an amorphous structure in addition to a solid solution structure. HEAFs inherit the high-entropy effect, hysteresis diffusion effect and severe lattice distortion of HEAs and tend to form single-phase solid solution structures and avoid the formation of brittle intermetallic compounds. At the same time, compared with the preparation methods of bulk high-entropy alloys, such as arc melting or induction melting, the cooling rate of high-entropy alloy film preparation methods is high, and it often shows the "rapid quenching" effect during the preparation process; thus, it is easy to form amorphous structures.

The phase structure of various high-entropy alloy films is not invariable, and the changes of element types and contents in high-entropy alloys affect the phase structure of HEAFs. In 2015, Braeckman et al. [39] found that with an increase in Nb content, the $Nb_xCoCrCuFeNi$ HEAFs changed from FCC to an amorphous structure. In 2018, Xing et al. [40] prepared high-entropy alloy films by co-sputtering a CrFeV target and an TaW target. With the increase in Ta and W element content, the films transformed from amorphous to BCC structure. In 2020, Fang et al. [41] found that the $CoCrFeMnNiV_x$ HEA films transformed from FCC to amorphous structure with an increase in V content.

The phase structure of high-entropy alloy films is affected not only by the change of element type and content in high-entropy alloys, but also by the nitridation and oxidation of high-entropy alloys. In 2004, Chen et al. [9] prepared FeCoNiCrCuAlMn and

FeCoNiCrCuAl$_{0.5}$ high-entropy alloy nitride films using a direct current magnetron sputtering technique and investigated the effect of the nitrogen flow rate on the phase composition and properties of the nitride films, which reflected that the nitride films gradually transformed to an amorphous state and the hardness was improved with the increase in nitrogen flow rate. In 2005, Chen et al. [42] investigated the effect of the nitrogen flow rate on the phase composition of Al$_2$CoCrCuFeNi and AlCrNiSiTi nitride films after changing the alloy composition. It was found that with the increase in nitrogen flow rate, the phase structure of Al$_2$CoCrCuFeNi nitride films changed from crystalline to amorphous, which is the same as that of AlCoCrCuFeMnNi and Al$_{0.5}$CoCrCuFeNi nitride films. In contrast, the metal film of AlCrNiSiTi was amorphous. With the increase in nitrogen content, the phase structure gradually changed from amorphous to a crystalline state. Subsequently, it was found that with the increase in nitrogen content, the phase structure of (Al$_{0.5}$CrFeNiTi$_{0.25}$)N$_x$ [11], (MoSiTiVZr)N$_x$ [43], (AlCrNbSiTiV)N [44], (FeCrVTa$_{0.4}$W$_{0.4}$)N$_x$ [45], (AlCrTiZrNb)N [46] and (AlCrTiZrHf)N [47] coatings changed from an amorphous structure to FCC structure. In 2007, Huang et al. [48] showed that AlCoCrCu$_{0.5}$FeNi high-entropy alloy films deposited using a radio frequency sputtering system were amorphous, and the introduction of O atoms transformed the AlCoCrCu$_{0.5}$NiFe oxide films into HCP. During the nitriding process, the phase structure transformation of the high-entropy alloy nitride films is closely related to the elements composing the high-entropy alloys. When more strong nitride-forming elements (e.g., Al, Cr, Ti, V, Zr, Nb, Mo, Hf, Ta, etc.) are present in the films, with the increase in nitrogen flow rate, the films change from amorphous structure to FCC structure. When more non-nitride forming elements (e.g., Co, Fe, Ni, Mn, Cu, etc.) are present, the films tend to transform from crystalline structure to amorphous structure.

In the process of preparing HEAFs, the microstructure with different grain size and orientation can be obtained by adjusting the experimental parameters. Next, the effect of sputtering parameters on the microstructure of thin films is summarized by taking the preparation of high-entropy alloy thin films using magnetron sputtering as an example.

The sputtering power affects the microstructure of HEAFs. In 2009, Dolique et al. [49] prepared AlCoCrCuFeNi high-entropy alloy metal films with direct current magnetron sputtering and determined that the sputtering power determines the composition and microstructure of the films. In 2020, Khan et al. [50] deposited AlCoCrCu$_{0.5}$FeNi high-entropy alloy films at 200, 250 and 300 W radio frequency power. The films were FCC + BCC solid solution structure at all sputtering powers. With the increase in sputtering power, the crystallinity of the films improved and the crystal size and surface roughness increased.

In addition to the sputtering power, the substrate temperature also affects the microstructure of the HEAFs. In 2016, Shi et al. [51] explored the phase structure of CoCrFeMnNi HEAFs at different substrate temperatures. When the substrate temperatures were 100, 200 and 300 °C, the deposited films were amorphous. At a substrate temperature of 400 and 500 °C, the deposited films were crystalline in structure. TaNbHfZr high-entropy alloy film was amorphous when deposited at room temperature. With the increase in substrate temperature, the film gradually crystallized and transformed into BCC phase [52]. The increase in substrate temperature was conducive to the increase in crystallinity.

The substrate bias affects the densities and phase structure of the films. In 2012, Shen et al. [53] found that the phase structure of (Al$_{1.5}$CrNb$_{0.5}$Si$_{0.5}$Ti)N$_x$ films was FCC structure under different substrate bias. As shown in the Figures 3 and 4, the film surface gradually transitioned from cauliflower-shaped to a smooth surface, the cross-section changed from columnar to dense morphology and the grain size decreased from 70 nm to 5 nm as the substrate bias voltage increased from 0 V to −150 V. The increase in substrate bias inhibited the grain growth. In 2020, Wang et al. [54] found that the AlCrSiNbZr nitride film was a mixture of FCC crystalline and amorphous phases at 0, −25, −50 and −75 V substrate bias, as shown in Figure 5. When the substrate bias increased from 0 to −50 V, the crystallinity of the film increased. Once the applied bias voltage exceeded −50 V, the crystallinity of the films began to decline. When the substrate bias reached −100 V, the film was almost amorphous. This is because the migration efficiency of adsorbed atoms on the surface of

the films increased and the oxygen content of the films decreased during the increase in the substrate bias from 0 to -50 V. The lattice defects and ion enhancement effects caused by the high-energy particle bombardment increased the proportion of amorphous phases when the substrate bias was increased from -50 to -100 V.
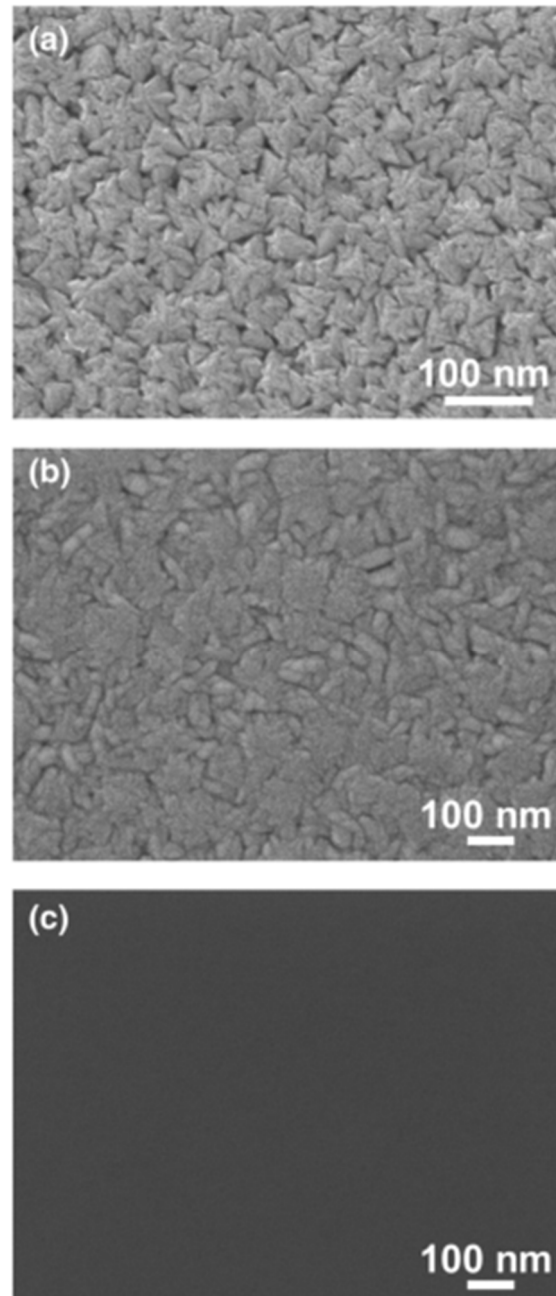
Figure 3. Plane-view SEM micrographs of $(Al_{1.5}CrNb_{0.5}Si_{0.5}Ti)N_x$ coatings deposited at substrate bias of (**a**) 0 V; (**b**) -50 V and (**c**) -150 V. Reprinted with permission from [53]. 2012, Elsevier.
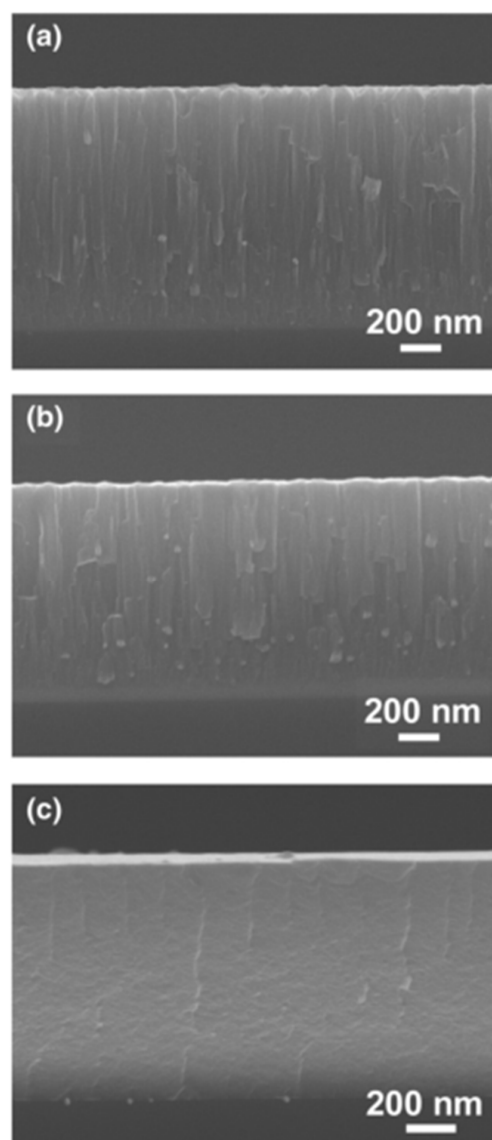
Figure 4. Cross-sectional SEM micrographs of $(Al_{1.5}CrNb_{0.5}Si_{0.5}Ti)N_x$ coatings deposited at substrate bias of (**a**) 0 V; (**b**) −50 V and (**c**) −150 V.. Reprinted with permission from [53]. 2012, Elsevier.
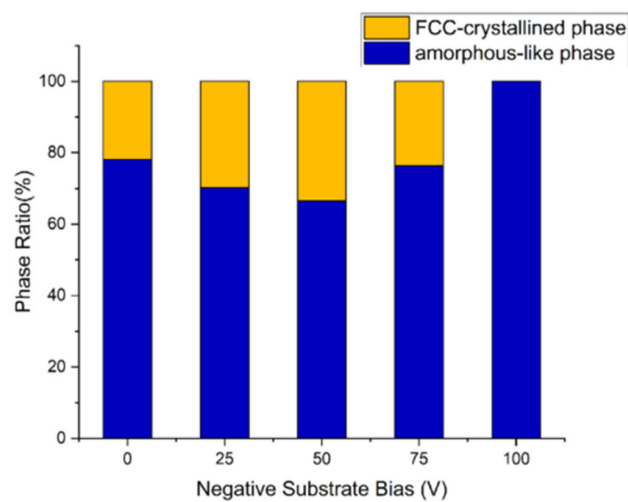
Figure 5. The correlated phase ratio of (AlCrSiNbZr)N film with different substrate biases. Reprinted with permission from [54]. 2020, Elsevier.

*3.2. Properties*

3.2.1. Hardness

High-entropy alloy films readily form nanocrystalline or amorphous structures, and thus exhibit a high hardness and elastic modulus that far exceed those of conventional films. Due to the combination of nanocrystalline and amorphous phase strengthening mechanisms, the maximum hardness of $W_{15.39}Ta_{38.81}Cr_{14.58}Fe_{15.45}Ni_{15.77}$ alloy film is 20.6 GPa [55], higher than that of most HEAFs. Compared with the single-phase FCC high-entropy alloy films, the hardness of the dual-phase high-entropy alloy films is higher. Cai et al. [56] studied the hardness of FCC/BCC dual-phase $Al_xCoCrCuFeNi$ HEAFs, with the maximum of 10.4 GPa.

High-entropy alloy nitride films, oxide films or carbide films are synthesized by adding a reactive gas, such as nitrogen, oxygen or methane, to the deposition process. The hardness of the prepared high-entropy alloy nitride films is high when nitrogen is added to alloys composed of strong nitride-forming elements. In some high-entropy alloy nitride film systems, the hardness exceeds 40 GPa, reaching the standard of a superhard film. In 2009, Huang et al. [44] prepared (AlCrNbSiTiV)N coatings by selecting six strong nitride-forming elements, Al, Cr, Nb, Si, Ti and V. The hardness of AlCrNbSiTiV coatings reached 41 GPa. In 2011, Cheng et al. [57] prepared $(AlCrMoTaTiZr)N_x$ coatings. The hardness could reach 40.2 GPa when the nitrogen flow ratio $R_N[N_2/(Ar + N_2)] = 40\%$. In 2012, Briac et al. [58] prepared TiZrNbHfTa high-entropy alloy nitride films using a multi-target co-sputtering method. The hardness was increased by about 10 GPa compared to the binary TiN film. In 2022, Li et al. [43] deposited $(MoSiTiVZr)N_x$ high-entropy alloy coatings. When the N content was 53.7 at.%, the coating had an ultra-hardness of 45.6 GPa. Figure 6 shows the relationship between the hardness and elastic modulus of common alloys and high-entropy alloy films. High-entropy alloy films show advantages in hardness and elastic modulus. HEAFs are mostly prepared with magnetron sputtering, which results in good film densities, strong bonding with the substrate and high film hardness. The reason for the high hardness of high-entropy alloy nitride films is that a large number of nitrogen elements exist in the film in the form of interstitial atoms, which reduces the Gibbs free energy of the system and causes serious lattice distortion.
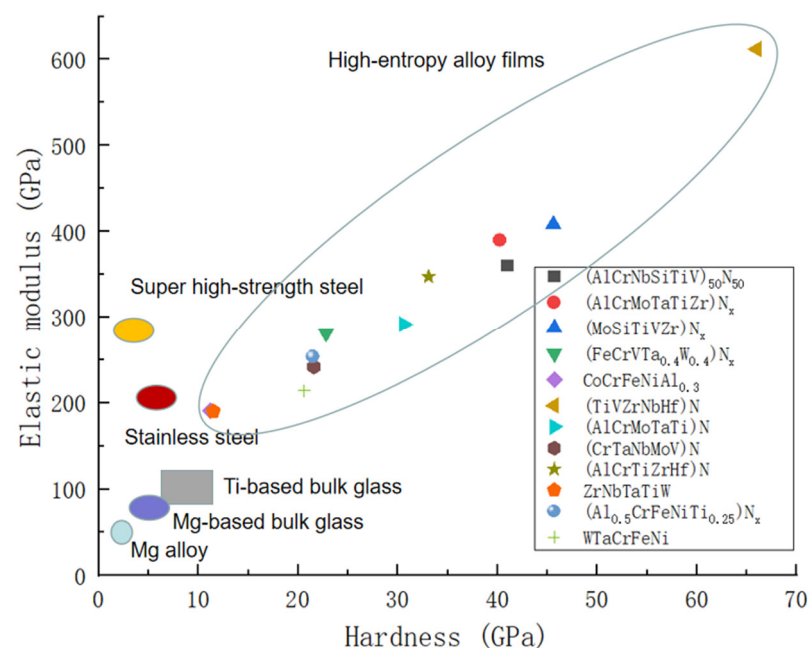
Figure 6. Relationship between hardness and elastic modulus for common alloys and high-entropy alloy films.

3.2.2. Corrosion Resistance

High-entropy alloy films have excellent corrosion resistance and can be widely used as corrosion-resistant coatings. The addition of aluminum can inhibit the pitting tendency of HEAFs. In 2017, Gao et al. [59] explored the corrosion behavior of $CoCrFeNiAl_{0.3}$ HEAFs at room temperature and in a 3.5 wt.% (weight percentage) NaCl solution. The corrosion potential of the high-entropy alloy films was slightly higher than that of 304 stainless steel and the corrosion current density was slightly lower. The critical pitting potential of 304 stainless steel was lower than that of the high-entropy alloy films and the passive zone was much larger. Compared with 304 stainless steel, $CoCrFeNiAl_{0.3}$ high-entropy alloy films had better local corrosion resistance. This is attributed to the presence of corrosion-resistant elements such as Ni, Co and Cr in the high-entropy alloy films and the uniform distribution of nanoparticles that contribute to the formation of dense oxide films.

The excellent corrosion resistance of the high-entropy alloy coatings depends on the corrosion-resistant elements such as Co, Mo, Ni and Cr contained in the coatings. In 2017, Qiu et al. [60] found that with the increase in Co content, $Al_2CrFeCo_xCuNiTi$ (x = 0, 0.5, 1.0, 1.5, 2.0) high-entropy alloy coatings had excellent corrosion resistance in H_2SO_4 and HCl solutions. This is because with the increase in Co content, the microstructure of the coatings became more homogeneous, and the passivation films formed on the alloy surface were more dense. $Al_2CrFeCo_xCuNiTi$ alloy coatings had no pitting in 0.5 mol/L H_2SO_4 solution, while pitting occurred in 0.5 mol/L HCl solution.

The addition of Mo improves the corrosion resistance of HEAFs in NaCl solution. In 2020, Liu et al. [61] found that $CoCrFeNiMo_x$ (x = 0.1, 0.2, 0.3) HEAFs had excellent corrosion resistance in 3.5% (mass fraction) NaCl solution. The $CoCrFeNiMo_{0.1}$ and $CoCrFeNiMo_{0.2}$ high-entropy alloy coatings were composed of the FCC phase, while the $CoCrFeNiMo_{0.3}$ high-entropy alloy coatings were composed of the FCC phase and the σ phase. With the increase in Mo content, the corrosion potential of the coatings moved forward and the corrosion current density decreased.

The introduction of excessive Ti atoms is not conducive to the improvement of corrosion resistance of high-entropy alloy coatings. In 2022, Liu et al. [62] investigated the effect of Ti content on the corrosion resistance of $CoCrFeMnNiTi_x$ (x = 0.25, 0.5, 0.75, 1.00, molar ratio) coatings. The coatings consisted of FCC solid solution phase and TiC particle phase. $Ti_{0.25}$ coating had the optimum corrosion resistance. The reason is that with the increase in the Ti content, the segregation of Ti element aggravated and the intergranular corrosion intensified.

In 2022, Huang et al. [14] investigated the effect of Cu content on the corrosion resistance of $AlCu_xNiTiZr_{0.75}$ (x = 1, 1.4, 2, 2.4, 2.8) high-entropy alloy films. The films were amorphous with homogeneous or columnar structure along the cross section, as shown in Figure 7. The introduction of Cu reduced the passivation ability of the films, resulting in a slight decrease in the corrosion resistance of the films.

Amorphous high-entropy alloy films tend to exhibit higher corrosion resistance among solid solution and amorphous structures. In 2016, Shi et al. [51] compared the corrosion resistance of 304 stainless steel and CoCrFeMnNi films deposited at different substrate temperatures (100, 200, 300, 400, 500 °C) at 1 mol/L H_2SO_4. The self-corrosion potential of 304 stainless steel was the most negative, and the self-corrosion potential of the film deposited when the substrate temperature is 100 °C was the most positive. The corrosion resistance of the CoCrFeMnNi HEAFs deposited at different temperatures were superior to that of 304 stainless steel. The HEAFs deposited at the substrate temperature of 100 °C are amorphous and therefore do not have the local organisational inhomogeneities such as grain boundaries and segregation that are characteristics of crystalline metals, which makes the amorphous structure films exhibit better corrosion resistance. When the substrate temperature gradually increases, the crystallinity of the films become better and transforms into a crystalline structure with more various defects. At the same time, the substrate temperature rises, and the films become increasingly rough, which eventually leads to decreased corrosion resistance of the films. In 2021, HEAF was tested in artificial seawater.

The corrosion resistance of the amorphous film was much higher than that of 304 stainless steel, and the corrosion current density was 4.68×10^{-9} A/cm^2, which was the effect of the amorphous structure and corrosion-resistant constituent elements. In 2022, Feng et al. [63] found that the current density of the AlTiVNb HEAF in a 3.5 wt.% NaCl solution was 4.9×10^{-8} A/cm^2 and the potential was -0.234 V. The corrosion resistance of AlTiVNb HEAFs was superior to that of 316L stainless steel. The superior corrosion resistance was attributed to the homogeneous amorphous structure. Table 2 shows the corrosion parameters of the high-entropy alloy coatings. It can be seen from the table that the corrosion rate of the amorphous high-entropy alloy coatings is lower.
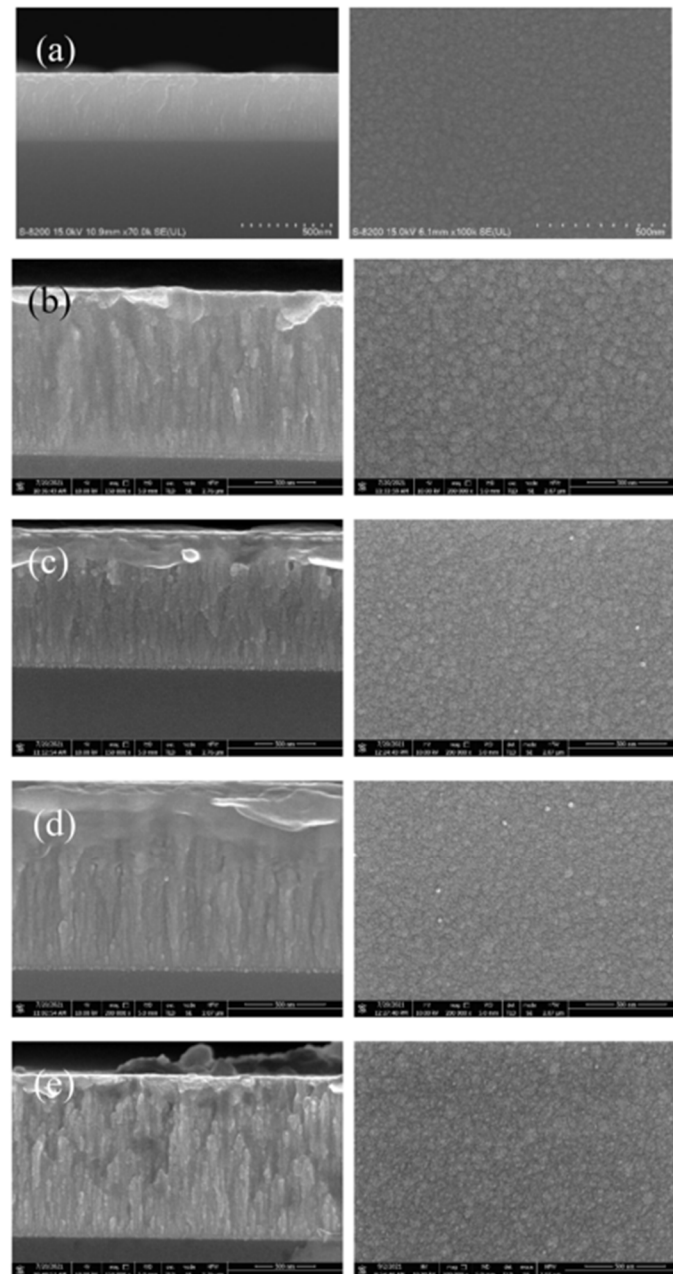
Figure 7. Cross-sectional SEM (left) and plane-view SEM micrographs (right) of AlCu$_x$NiTiZr$_{0.75}$ films: (**a**) AlCuNiTiZr$_{0.75}$, (**b**) AlCu$_{1.4}$NiTiZr$_{0.75}$, (**c**) AlCu$_2$NiTiZr$_{0.75}$, (**d**) AlCu$_{2.4}$NiTiZr$_{0.75}$, (**e**) AlCu$_{2.8}$NiTiZr$_{0.75}$. Reprinted with permission from [14]. 2022, Elsevier.

Table 2. Corrosion parameters of high-entropy alloy coatings.

Coating	Phase Composition	Corrosion Rates (mm/A)	Corrosion Potentials (V)	Corrosion Current Density ($\mu A \cdot cm^{-2}$)	Reference
$Al_{0.3}CoCrFeNi$	FCC	1.2×10^{-3}	-0.451	0.103	[59]
$Al_2CrFeCo_{0.5}CuNiTi$		4.56×10^{-3}	-0.25	0.39	[60]
$CoCrFeNiMo_{0.3}$	FCC+ σ	4.95×10^{-2}	-0.66	4.23	[61]
$CoCrFeMnNiTi_{0.25}$	FCC + TiC	5.38×10^{-2}	-0.490	4.6	[62]
$AlCuNiTiZr_{0.75}$	Amorphous	9.0×10^{-4}	-0.31	7.69×10^{-2}	[14]
$CoCrFeMnNi$	FCC	0.164	-0.257	14	[51]
$AlTiVNb$	Amorphous	5.73×10^{-4}	-0.234	4.9×10^{-2}	[63]
$VAlTiCrSi$	Amorphous	5.48×10^{-5}	-0.285	4.68×10^{-3}	[64]
$AlCoCrFeNiSi_x$	BCC	3.42×10^{-3}	-0.31	0.292	[65]
$AlCoCrFeNiCu$	FCC + BCC	0.03	-0.601	2.56	[66]
$Al_2CoCrCuFeNiTi$	FCC + BCC + Laves	2.69×10^{-4}	-0.52	2.3×10^{-2}	[67]

3.2.3. Wear Resistance

In addition to corrosion resistance, wear resistance is also one of the indicators to measure the service life of materials. The wear resistance of the films is mainly related to the microstructure, hardness, friction coefficient and wear rate. According to the Archard law, the wear resistance of the material is proportional to the hardness [68]. Smaller surface roughness and higher hardness can lead to a lower friction coefficient and wear rate of the films, which is conducive to the improvement of wear resistance of the high-entropy alloy films.

In 2017, Guo et al. [69] analyzed the wear resistance of high-melting-point $AlCrFeMoNb_xTiW$ (x = 1, 3, 5 and 7) high-entropy alloy coatings with industrial annealed $W_6Mo_5Cr_4V_2$ tool steel as the substrate. With the increase in Nb content, the hardness of the coatings increased, and the friction coefficient and wear rate decreased. Due to the increase in Nb content, the content of carbides and intermetallic compounds in the coatings increased significantly, and the hardness increased, which reduced the plastic contact between friction pairs and improved the adhesive wear resistance. In addition, the overall hardness of each Nb_x coatings is much higher than that of the substrate. $AlCrFeMoNb_xTiW$ high-entropy alloy coatings can be used to improve the surface wear resistance of high-speed cutting tools.

CoCrFeNi high-entropy alloy is a single FCC solid solution structure with poor hardness and wear resistance. The hardness and wear resistance of the films are generally improved by introducing other elements. In 2019, Liu et al. [70] investigated the wear resistance of $FeCoCrNiB_x$ (x = 0.5, 1 and 1.5) coatings. With the increase in B content, the microstructure was refined and the hardness and wear resistance were increased. Among the three coatings, $FeCoCrNiB_{1.5}$ HEA coating had the smallest wear volume and the highest hardness of 1025 $HV_{0.2}$, which was higher than the substrate material Q245R. The improvement of wear resistance was attributed to the formation of borides. $FeCoCrNiB_x$ high-entropy alloy coatings have potential application in mild steel wear-resistant structures. In 2020, Wang et al. [71] analyzed the wear resistance of $CoCrFeNiMo_x$ (x = 0.1, 0.2 and 0.3) high-entropy alloy coatings. The hardness and wear resistance of the coatings were continuously increased and the friction factor and wear rate were continuously reduced by the effect of Mo elements. The σ phase was generated to prevent plastic deformation and wear-scar development of the coatings, which enhances the wear resistance of the coatings.

The soft FCC structure is transformed into hard BCC structure by introducing N element for strengthening. In 2020, Sha et al. [72] deposited $(CoCrFeMnNi)N_x$ high-entropy alloy coatings under different nitrogen flow rates (4, 8, 15, 25 sccm). The N atoms could

induce the transformation of the films from FCC to BCC structure and greatly improve the hardness and wear resistance of the films. In the same year, Cui et al. [47] found that due to the formation of the nitride ceramic phase, the friction coefficient of (AlCrTiZrHf)N high-entropy alloy nitride films was lower than that of AlCrTiZrHf high-entropy alloy metal film. The nitrided ceramic phase was characterized by high hardness, good wear resistance and low friction coefficient.

Based on the cooling rate during film deposition, Xing et al. [73] modified the thermodynamic parameter Ω, which predicts the phase formation of the bulk alloy S, to Ω_T. The Ω_T and δ of $(CrMnFeHf)_{7.14}(TiTaV)_{23.81}$ alloy are 5.91% and 5.46%, respectively, which are consistent with the formation law of solid solution. The composition is in the solid solution and intermetallic regions of the Ω_T-δ phase diagram. While magnetron sputtering is a non-equilibrium process, the CrMnFeHfTiTaV alloy film prepared using magnetron sputtering usually has a strong glass-forming ability ($\Omega_T \leq 1.1$) and tends to form an amorphous phase, which is the orange area marked in Figure 8. CrFeHfMnTiTaV alloy film can improve the surface properties of 304 stainless steel and provide sliding wear protection from room temperature to 500 °C for 304 stainless steel, which is suitable for a high-temperature protective film.
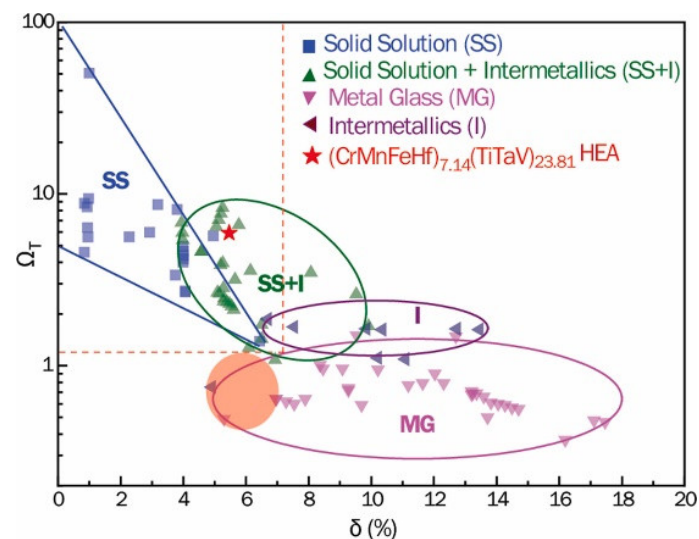
Figure 8. Ω_T-δ diagram for HEAs and CrMnFeHfTiTaV HEA. The orange-filled circle marks the possible area, where the Ω_T of $(CrMnFeHf)_{7.14}(TiTaV)_{23.81}$ is located in [73].

3.2.4. Thermal Stability

Currently, ceramics are the ideal diffusion barrier material due to the fact that the failure temperature of metal diffusion barriers is significantly lower than that of ceramic diffusion barriers. In 2011, Tsai [74] found that the effective temperature of NbSiTaTiZr high-entropy alloy diffusion barrier is equivalent to that of many ceramic diffusion barriers. NbSiTaTiZr high-entropy alloy diffusion barrier can prevent the mutual diffusion between Cu and Si for 30 min at 800 °C. In 2020, Jiang et al. [75] found that AlCrTaTiZr/AlCrTaTiZr-N alloy films could also block the diffusion of copper at 900 °C, and no copper silicide formation.

In 2016, Zhang et al. [76] conducted high-temperature oxidation tests on $FeCoCr_xNiB$ (x = 0.5~3) high-entropy alloy coatings with different Cr contents at 900 °C. The oxidation kinetics curve of $FeCoCr_xNiB$ high-entropy alloy coatings with different Cr contents basically conformed to the parabolic law. With the increase in Cr content, the oxidation rate of the coating decreased and the oxidation resistance of the coating increased. In 2021, Ma et al. [77] studied the effect of Si on the oxidation resistance of $CoCr_2FeNb_{0.5}Ni$ high-entropy alloy coatings at 800 °C. As shown in Figure 9, the oxidation kinetics of $Cr_2FeNb_{0.5}Ni$ and $Cr_2FeNb_{0.5}NiSi_{0.2}$ HEAs coatings at 800 °C followed the parabolic law, and the oxidation rate constant decreased with the addition of Si. Table 3 shows the parabolic rate constant Kp of the high-entropy alloy coatings. The smaller Kp, the better

high-temperature oxidation resistance and thermal stability. At low temperatures, Kp lies at a low level. As the temperature increases, the Kp value increases. The addition of Al reduces the Kp value, indicating that the addition of Al significantly improves the high-temperature oxidation resistance of the coatings.
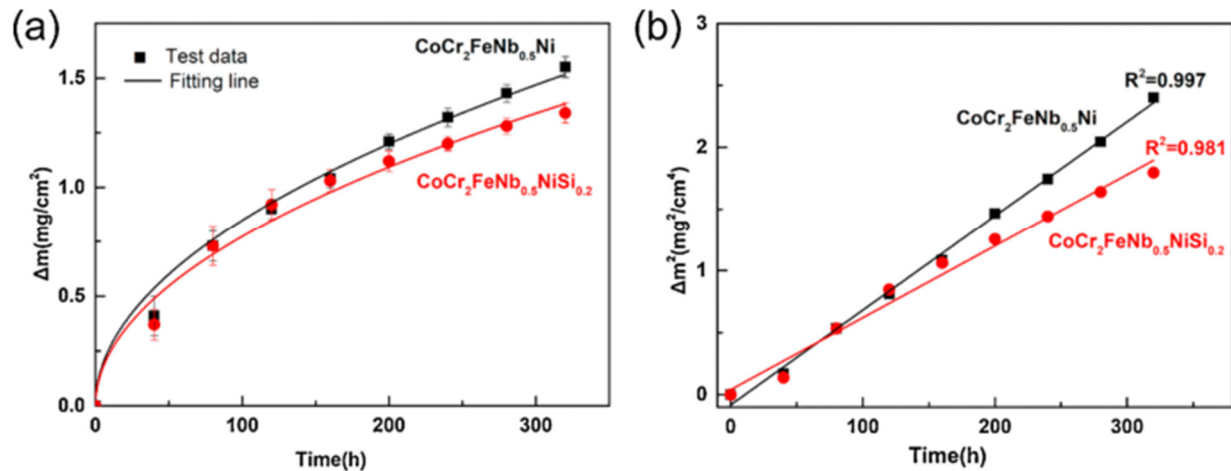
Figure 9. Oxidation kinetics of $Cr_2FeNb_{0.5}Ni$ and $Cr_2FeNb_{0.5}Ni$ coating at 800 °C: (**a**) Weight gains plots; (**b**) oxidation rate constant. Reprinted with permission from [77]. 2021, Elsevier.

Table 3. Parabolic rate constants of HEA coatings.

Alloy	Kp ($g^2 \cdot cm^{-4} \cdot s^{-1}$)	Temperature (°C)	Reference
$AlCoCrFeNiTi_{0.5}$	3.06×10^{-13} 2.14×10^{-12}	700 800	[78]
FeCoCrNiMo	4.92×10^{-10}	1000	[79]
$FeCoCrNiAl_{0.3}$	1.627×10^{-13}	950	[80]
$FeCoCrNiAl_{0.5}$	1.056×10^{-13}	950	[80]
$FeCoCrNiAl_{0.7}$	5.681×10^{-14}	950	[80]
FeCoCrNiAl	3.064×10^{-14}	950	[80]
AlCoCrFeNi	1.976×10^{-15} 1.285×10^{-14} 1.701×10^{-14}	800 900 1000	[81]

3.2.5. Magnetic Properties

The magnetic research of high-entropy alloys shows that high-entropy alloys can meet the requirements of soft magnetic materials with high saturation magnetisation, low coercivity and high resistivity. The excellent magnetic properties of high-entropy alloy films are attributed to the presence of magnetic elements such as Fe, Co and Ni. In 2011, Yao et al. [38] found that Nd-Fe-Co-Ni-Mn HEAFs have very low coercivity at both ambient and low temperatures and easily reach saturation magnetization. With the decrease in temperature, the saturation magnetization continues to increase. In 2023, Luo et al. [82] found that $Fe_{0.18}Co_{0.36}Ni_{0.21}Al_{0.10}Cr_{0.15}$ HEAFs annealed at 400~800 °C can effectively improve the saturation magnetization. The alloy is annealed at 800 °C to obtain optimum properties, which can be applied to functional soft magnetic materials. Yao et al. [37] deposited $Bi_{19.3}Fe_{20.7}Co_{18.8}Ni_{22.0}Mn_{19.2}$ amorphous films at constant potential. The annealed alloy structure is mainly composed of FCC. The deposited alloys show soft magnetic properties, while the annealed alloys exhibit hard magnetic properties.

3.2.6. Other Properties

In 2018, Xing et al. [40] discovered the potential photothermal conversion material $Cr_6Fe_6V_6Ta_{42}W_{40}$ with a solar absorption of 81.94%. The variation in solar absorptance was positively correlated with the surface roughness. In 2022, Huang et al. [83] employed the substrate prestrain method to fabricate wrinkle-structured $Zr_{52}Ti_{34}Nb_{14}$ multiple-basis-element alloy films as biocompatible materials. The variations in film thickness and substrate prestraining can precisely control the amplitude and wavelength of the wrinkled structure in the range from micrometers to nanometers.

4. Discussion

The shortcomings of previous studies and the future directions of high-entropy alloy films include the following aspects. The law of phase formation plays a guiding role in the design and applications of HEAFs. The phase formation law of bulk alloys is not suitable for the prediction of phase structure of HEAFs, so it is necessary to establish the phase formation law of films. Previous studies have mostly focused on the influence of the magnetron sputtering process parameters on the microstructure and properties. The influence of the process parameters on the structure and properties of HEAFs still needs to be improved. At present, the preparation technology of HEAFs has shortcomings, and it is still necessary to explore new methods for preparing HEAFs. Compared with conventional alloys, HEAs contain a large number of components and the interaction between components is more complex. High-throughput experiments can provide a large amount of basic data for the material database, facilitating the rapid search of the "process–composition–structure–property" intrinsic law and accelerating the selection and optimization of materials. The thin-film methods of realizing the required material composition include the co-deposition method, the discrete template coating method, the continuous template coating method and the combination coating method of discrete template and continuous template. The laser additive method has high technological accuracy and can realize the rapid preparation of sample libraries of millimeter and centimeter scales. Using machine learning technology to analyze data can improve the efficiency of HEAF composition design and reduce the development cost. Most studies of HEAFs have been carried out at room or high temperatures, lacking complex operating conditions such as low temperatures. Future work should develop research on high-entropy alloy films at extremely low temperatures and broaden the temperature range of HEAFs. Despite the excellent properties of HEAFs, problems such as high production costs and immature processes have led to few practical applications of high-entropy alloy films.

5. Conclusions

The solidification rate of bulk high-entropy alloy materials prepared with vacuum arc melting or induction melting is usually not high. Usually there are more kinds of elements in HEAs, and various elements will inevitably lead to segregation due to the large difference in density, which tends to cause a non-uniform distribution of the high-entropy alloy composition. High-entropy alloys contain a variety of expensive elements with high content and high cost, which seriously limits their engineering applications. How to put high-entropy alloys into engineering applications is still a challenge. HEAFs can better realize the practical application of HEAs.

The low-dimensional characteristics of the HEAFs make it possible for the films to be used in thin, light, portable electronic devices and even microelectronics with higher precision requirements [84]. The wrinkle-structured multiple-basis-element alloy films can broaden the application of the alloy films in the field of flexible materials, and can be applied to smart windows [83]. In addition, high-entropy alloy films have shown profound development prospects in the fields of corrosion protection, diffusion barrier and photothermal conversion coatings.

References

1. Yeh, J.W.; Chen, S.K.; Lin, S.J.; Gan, J.Y.; Chin, T.S.; Shun, T.T.; Tsau, C.H.; Chang, S.Y. Nanostructured High-Entropy Alloys with Multiple Principal Elements: Novel Alloy Design Concepts and Outcomes. *Adv. Eng. Mater.* **2004**, *6*, 299–303. [CrossRef]
2. Cantor, B.; Chang, I.T.H.; Knight, P.; Vincent, A.J.B. Microstructural development in equiatomic multicomponent alloys. *Mater. Sci. Eng. A* **2004**, *375–377*, 213–218. [CrossRef]
3. Guo, N.N.; Gao, X.J.; Zhu, G.M.; Fang, X.Y. Research Progress of Refractory High-entropy Alloys. *Hot Work. Technol.* **2021**, *50*, 1–4.
4. Zhou, P.Y.; Liu, H.X.; Zhang, X.W.; Hao, X.H.; Wang, Y.Y.; Chen, L. Research Progress of Light-weight High-entropy Alloy. *China Surf. Eng.* **2021**, *34*, 265–274. (In Chinese)
5. Cui, K.X.; Liaw, P.K.; Zhang, Y. Cryogenic-Mechanical Properties and Applications of Multiple-Basis-Element Alloys. *Metals* **2022**, *12*, 2075. [CrossRef]
6. Jiao, W.N.; Lu, Y.P.; Cao, Z.Q.; Wang, T.M.; Li, T.J.; Yin, G.M. Progress and Prospect of Eutectic High Entropy Alloys. *Spec. Cast. Nonferrous Alloys* **2022**, *42*, 265–274.
7. Zhang, Y.; Yan, X.H.; Liao, W.B.; Zhao, K. Effects of Nitrogen Content on the Structure and Mechanical Properties of $(Al_{0.5}CrFeNiTi_{0.25})N_x$ High-Entropy Films by Reactive Sputtering. *Entropy* **2018**, *20*, 624. [CrossRef]
8. Liao, W.B.; Lan, S.; Gao, L.B.; Zhang, H.T.; Xu, S.; Song, J.; Wang, X.L.; Lu, Y. Nanocrystalline high-entropy alloy ($CoCrFeNiAl_{0.3}$) thin-film coating by magnetron sputtering. *Thin Solid Films* **2017**, *638*, 383–388. [CrossRef]
9. Chen, T.K.; Shun, T.T.; Yeh, J.W.; Wong, M.S. Nanostructured nitride films of multi-element high-entropy alloys by reactive DC sputtering. *Surf. Coat. Technol.* **2004**, *188–189*, 193–200. [CrossRef]
10. An, Z.N.; Jia, H.L.; Wu, Y.Y.; Rack, P.D.; Patchen, A.D.; Liu, Y.Z.; Ren, Y.; Li, N.; Liaw, P.K. Solid-Solution CrCoCuFeNi High-Entropy Alloy Thin Films Synthesized by Sputter Deposition. *Mater. Res. Lett.* **2015**, *3*, 203–209. [CrossRef]
11. Khan, N.A.; Akhavan, B.; Zhou, H.R.; Chang, L.; Wang, Y.; Sun, L.X.; Bilek, M.M.; Liu, Z.W. High entropy alloy thin films of $AlCoCrCu_{0.5}FeNi$ with controlled microstructure. *Appl. Surf. Sci.* **2019**, *495*, 143560–143568. [CrossRef]
12. Braeckman, B.R.; Boydens, F.; Hidalgo, H.; Dutheil, P.; Jullien, M.; Thomann, A.L.; Depla, D. High entropy alloy thin films deposited by magnetron sputtering of powder targets. *Thin Solid Films* **2015**, *580*, 71–76. [CrossRef]
13. Feng, X.G.; Tang, G.Z.; Sun, M.R.; Ma, X.X.; Wang, L.Q.; Yukimura, K. Structure and properties of multi-targets magnetron sputtered ZrNbTaTiW multi-elements alloy thin films. *Surf. Coat. Technol.* **2013**, *228*, S424–S427. [CrossRef]
14. Huang, K.; Wang, G.M.; Qing, H.W.; Chen, Y.G.; Guo, H.B. Effect of Cu content on electrical resistivity, mechanical properties and corrosion resistance of $AlCu_xNiTiZr_{0.75}$ high entropy alloy films. *Vacuum* **2022**, *195*, 110695–110703. [CrossRef]
15. Yan, X.H.; Zhang, Y. Preparation and forming process of high-entropy alloy. *J. Netshape Form. Eng.* **2022**, *14*, 19–27. (In Chinese)
16. Zhang, H.; He, Y.Z.; Pan, Y.; He, Y.S.; Shin, K.S. Synthesis and Characterization of $NiCoFeCrAl_3$ High Entropy Alloy Coating by Laser Cladding. *Adv. Mater. Res.* **2010**, *97–101*, 1408–1411. [CrossRef]
17. Zhang, H.; Pan, Y.; He, Y.Z.; Jiao, H.S. Microstructure and properties of 6FeNiCoSiCrAlTi high-entropy alloy coating prepared by laser cladding. *Appl. Surf. Sci.* **2011**, *257*, 2259–2263. [CrossRef]
18. Zhang, H.; Pan, Y.; He, Y.Z. Synthesis and characterization of FeCoNiCrCu high-entropy alloy coating by laser cladding. *Mater. Des.* **2011**, *32*, 1910–1915. [CrossRef]
19. Zhang, H.; Pan, Y.; He, Y.S. Laser cladding $FeCoNiCrAl_2Si$ high-entropy alloy coating. *Acta Metall. Sin.* **2011**, *47*, 1075–1079. (In Chinese)
20. Zhang, H.; He, Y.Z.; Pan, Y. Enhanced hardness and fracture toughness of the laser-solidified $FeCoNiCrCuTiMoAlSiB_{0.5}$ high-entropy alloy by martensite strengthening. *Scr. Mater.* **2013**, *69*, 342–345. [CrossRef]
21. Qiu, X.W.; Zhang, Y.P.; Liu, C.G. Microstructure and properties of $Al_2CrFeCo_xCuNiTi$ high-entropy alloy coating prepared by laser cladding. *Mater. Sci. Eng. Powder Metall.* **2013**, *18*, 735–740. (In Chinese)
22. Zhou, F.; Liu, Q.B.; Zheng, B. Effect of Si, Al on the microstructure and properties of MoFeCrTiW high-entropy alloy coating prepared by laser cladding. *High Power Laser Part. Beams* **2015**, *27*, 272–277. (In Chinese)
23. Li, Q.Y.; Li, D.C.; Zhang, H.; Zhang, A.F.; Liang, J.Y.; Wang, X.L.X.; Yan, H.Q. Study on the microstructure and strength of NbMoTaTi refractory high-entropy alloy deposited by laser melting. *Aeronaut. Manuf. Technol.* **2018**, *61*, 61–67. (In Chinese)
24. Wang, H.L.; Guo, Y.X.; Lan, H.W.; Liu, Q.B.; Zhou, F. Effect of Spot Type on Microstructure and Properties of MoFeCrTiWAlNb Refractory High-entropy Alloy Coating Fabricated by Laser Cladding. *Surf. Technol.* **2019**, *48*, 130–137. (In Chinese)

25. Ma, M.X.; Liu, Y.X.; Gu, Y.; Ye, X.Y.; Zhang, W.M.; Zhong, M.L.; Liu, W.J. Synthesis of AlxCoCrNiMo high entropy alloy coatings by laser cladding. *Appl. Laser* **2010**, *30*, 433–437. (In Chinese)

26. Weng, Z.Q.; Dong, G.; Zhang, Q.L.; Guo, S.R.; Yao, J.H. Effects of annealing on microstructure and properties of FeCrNiCoMn high-entropy alloy coating prepared by laser cladding. *Chin. J. Laser* **2014**, *41*, 65–70. (In Chinese)

27. Katakam, S.; Joshi, S.S.; Mridha, S.; Mukherjee, S.; Dahotre, N.B. Laser assisted high entropy alloy coating on aluminum: Microstructural evolution. *J. Appl. Phys.* **2014**, *116*, 104906–104912. [CrossRef]

28. Qiu, X.W.; Zhang, Y.P.; Liu, C.G. Effect of Ti content on structure and properties of Al$_2$CrFeNiCoCuTi$_x$ high-entropy alloy coatings. *J. Alloys Compd.* **2014**, *585*, 282–286. [CrossRef]

29. Yue, T.M.; Xie, H.; Lin, X.; Yang, H.O.; Meng, G.H. Solidification behaviour in laser cladding of AlCoCrCuFeNi high-entropy alloy on magnesium substrates. *J. Alloys Compd.* **2014**, *587*, 588–593. [CrossRef]

30. Shon, Y.; Joshi, S.S.; Katakam, S.; Shanker Rajamure, R.; Dahotre, N.B. Laser additive synthesis of high entropy alloy coating on aluminum: Corrosion behavior. *Mater. Lett.* **2015**, *142*, 122–125. [CrossRef]

31. Huang, C.; Zhang, Y.Z.; Vilar, R.; Shen, J.Y. Dry sliding wear behavior of laser clad TiVCrAlSi high entropy alloy coatings on Ti–6Al–4V substrate. *Mater. Des.* **2012**, *41*, 338–343. [CrossRef]

32. Zhang, Y.Y.; Zhang, Z.B.; Yao, W.; Liang, X.B. Research status and prospects of high-entropy alloy thin film. *Surf. Technol.* **2021**, *50*, 117–129. (In Chinese)

33. Cropper, M.D. Thin films of AlCrFeCoNiCu high-entropy alloy by pulsed laser deposition. *Appl. Surf. Sci.* **2018**, *455*, 153–159. [CrossRef]

34. Lu, T.W.; Feng, C.S.; Wang, Z.; Liao, K.W.; Xie, Y.Z.; Hu, J.G.; Liao, W.B. Microstructures and mechanical properties of CoCrFeNiAl$_{0.3}$ high-entropy alloy thin films by pulsed laser deposition. *Appl. Surf. Sci.* **2019**, *494*, 72–79. [CrossRef]

35. Liao, W.B.; Wu, Z.X.; Lu, W.J.; He, M.J.; Wang, T.; Guo, Z.X.; Huang, J.J. Microstructures and mechanical properties of CoCrFeNiMn high-entropy alloy coatings by detonation spraying. *Intermetallics* **2021**, *132*, 107138–107146. [CrossRef]

36. Batraev, I.S.; Ulianitsky, V.Y.; Sova, A.A.; Samodurova, M.N.; Trofimov, E.A.; Pashkeev, K.Y.; Malikov, A.G.; Dudina, D.V.; Ukhina, A.V. A Feasibility Study of High-Entropy Alloy Coating Deposition by Detonation Spraying Combined with Laser Melting. *Materials* **2022**, *15*, 4532. [CrossRef]

37. Yao, C.Z.; Zhang, P.; Liu, M.; Li, G.R.; Ye, J.Q.; Liu, P.; Tong, Y.X. Electrochemical preparation and magnetic study of Bi-Fe-Co-Ni-Mn high entropy alloy. *Electrochim. Acta* **2008**, *53*, 8359–8365. [CrossRef]

38. Yao, C.Z.; Ma, H.X.; Tong, Y.X. Electrochemical preparation and magnetic properties of amorphous nano Nd-Fe-Co-Ni-Mn high-entropy alloy film. *Chin. J. Appl. Chem.* **2011**, *28*, 1189–1194.

39. Braeckman, B.R.; Depla, D. Structure formation and properties of sputter deposited Nb$_x$-CoCrCuFeNi high entropy alloy thin films. *J. Alloys Compd.* **2015**, *646*, 810–815. [CrossRef]

40. Xing, Q.; Ma, J.; Wang, C.; Zhang, Y. High-Throughput Screening Solar-Thermal Conversion Films in a Pseudobinary (Cr, Fe, V)-(Ta, W) System. *ACS Comb. Sci.* **2018**, *20*, 602–610. [CrossRef]

41. Fang, S.; Wang, C.; Li, C.L.; Luan, J.H.; Jiao, Z.B.; Liu, C.T.; Hsueh, C.H. Microstructures and mechanical properties of CoCrFeMnNiV high entropy alloy films. *J. Alloys Compd.* **2020**, *820*, 153388–153395. [CrossRef]

42. Chen, T.K.; Wong, M.S.; Shun, T.T.; Yeh, J.W. Nanostructured nitride films of multi-element high-entropy alloys by reactive DC sputtering. *Surf. Coat. Technol.* **2005**, *200*, 1361–1365. [CrossRef]

43. Li, J.C.; Chen, Y.J.; Zhao, Y.M.; Shi, X.W.; Wang, S.; Zhang, S. Super-hard (MoSiTiVZr)N$_x$ high-entropy nitride coatings. *J. Alloys Compd.* **2022**, *926*, 166807–166817. [CrossRef]

44. Huang, P.K.; Yeh, J.W. Effects of nitrogen content on structure and mechanical properties of multi-element (AlCrNbSiTiV)N coating. *Surf. Coat. Technol.* **2009**, *203*, 1891–1896. [CrossRef]

45. Wang, Z.X.; Zhang, Y. Microstructure and properties of FeCrVTa$_{0.4}$W$_{0.4}$ high-entropy alloy nitride films. *Chin. J. Eng.* **2021**, *43*, 684–692. (In Chinese)

46. Huang, C.K.; Li, W.; Liu, P.; Zhang, K.; Chen, X.H.; Ma, F.C.; Liu, X.K. Synthesis and mechanical properties of (AlCrTiZrNb)N high entropy alloy films grown by RF magnetron sputtering. *Chin. J. Vac. Sci. Technol.* **2018**, *38*, 487–493. (In Chinese)

47. Cui, P.P.; Li, W.; Liu, P.; Zhang, K.; Ma, F.C.; Chen, X.H.; Feng, R.; Liaw, P.K. Effects of nitrogen content on microstructures and mechanical properties of (AlCrTiZrHf)N high-entropy alloy nitride films. *J. Alloys Compd.* **2020**, *834*, 155063–155070. [CrossRef]

48. Huang, Y.S.; Chen, L.; Lui, H.W.; Cai, M.H.; Yeh, J.W. Microstructure, hardness, resistivity and thermal stability of sputtered oxide films of AlCoCrCu$_{0.5}$NiFe high-entropy alloy. *Mater. Sci. Eng. A* **2007**, *457*, 77–83. [CrossRef]

49. Dolique, V.; Thomann, A.L.; Brault, P.; Tessier, Y.; Gillon, P. Complex structure/composition relationship in thin films of AlCoCrCuFeNi high entropy alloy. *Mater. Chem. Phys.* **2009**, *117*, 142–147. [CrossRef]

50. Khan, N.A.; Akhavan, B.; Zhou, C.F.; Zhou, H.R.; Chang, L.; Wang, Y.; Liu, Y.P.; Fu, L.; Bilek, M.M.; Liu, Z.W. RF magnetron sputtered AlCoCrCu$_{0.5}$FeNi high entropy alloy (HEA) thin films with tuned microstructure and chemical composition. *J. Alloys Compd.* **2020**, *836*, 155348–155357. [CrossRef]

51. Shi, Y.Y.; Luo, Y.C.; Zhang, G.Q. Deposition and corrosion properties of FeNiCoCrMn high entropy alloy films under different substrate temperature. *Met. Funct. Mater.* **2016**, *23*, 35–39. (In Chinese)

52. Song, B.R.; Li, Y.H.; Cong, Z.H.; Li, Y.X.; Song, Z.X.; Chen, J. Effects of deposition temperature on the nanomechanical properties of refractory high entropy TaNbHfZr films. *J. Alloys Compd.* **2019**, *797*, 1025–1030. [CrossRef]

53. Shen, W.J.; Tsai, M.H.; Chang, Y.S.; Yeh, J.W. Effects of substrate bias on the structure and mechanical properties of $(Al_{1.5}CrNb_{0.5}Si_{0.5}Ti)N_x$ coatings. *Thin Solid Films* **2012**, *520*, 6183–6188. [CrossRef]

54. Wang, J.J.; Chang, S.Y.; Ouyang, F.Y. Effect of substrate bias on the microstructure and properties of (AlCrSiNbZr) N_x high entropy nitride thin film. *Surf. Coat. Technol.* **2020**, *393*, 125796–125806. [CrossRef]

55. Li, Y.S.; Ma, J.; Liaw, P.K.; Zhang, Y. Exploring the amorphous phase formation and properties of W-Ta-(Cr, Fe, Ni) high-entropy alloy gradient films via a high-throughput technique. *J. Alloys Compd.* **2022**, *913*, 165294–165303. [CrossRef]

56. Cai, Y.P.; Wang, G.J.; Ma, Y.J.; Cao, Z.H.; Meng, X.K. High hardness dual-phase high entropy alloy thin films produced by interface alloying. *Scr. Mater.* **2019**, *162*, 281–285. [CrossRef]

57. Cheng, K.H.; Lai, C.H.; Lin, S.J.; Ye, J.W. Structural and mechanical properties of multi-element $(AlCrMoTaTiZr)N_x$ coatings by reactive magnetron sputtering. *Thin Solid Films* **2011**, *519*, 3185–3190. [CrossRef]

58. Braic, V.; Vladescu, A.; Balaceanu, M.; Luculescu, C.R.; Braic, M. Nanostructured multi-element (TiZrNbHfTa)N and (TiZrNbHfTa)C hard coatings. *Surf. Coat. Technol.* **2012**, *211*, 117–121. [CrossRef]

59. Gao, L.B.; Liao, W.B.; Zhang, H.T.; Surjadi, J.; Sun, D.; Lu, Y. Microstructure, Mechanical and Corrosion Behaviors of $CoCrFeNiAl_{0.3}$ High Entropy Alloy (HEA) Films. *Coatings* **2017**, *7*, 156. [CrossRef]

60. Qiu, X.W.; Wu, M.J.; Liu, C.G.; Zhang, Y.P.; Huang, C.X. Corrosion performance of $Al_2CrFeCo_xCuNiTi$ high-entropy alloy coatings in acid liquids. *J. Alloys Compd.* **2017**, *708*, 353–357. [CrossRef]

61. Liu, Q.; Wang, X.Y.; Huang, Y.B.; Xie, L.; Xu, Q.; Li, L.H. Effect of Molybdenum Content on Microstructure and Corrosion Resistance of CoCrFeNiMo High Entropy Alloy. *Chin. J. Mater. Res.* **2020**, *34*, 868–874. (In Chinese)

62. Liu, H.; Gao, Q.; Man, J.X.; Li, X.J.; Yang, H.F.; Hao, J.B. Microstructure and Properties of $CoCrFeMnNiTi_x$ High-Entropy Alloy Coating by Laser Cladding. *Chin. J. Lasers* **2022**, *49*, 18–29. (In Chinese)

63. Feng, X.; Feng, C.; Lu, Y. A Lightweight AlTiVNb High-Entropy Alloy Film with High Strength-Ductility Synergy and Corrosion Resistance. *Materials* **2022**, *15*, 8568. [CrossRef] [PubMed]

64. Zheng, S.J.; Cai, Z.B.; Pu, J.B.; Zeng, C.; Wang, L.P. Passivation behavior of VAlTiCrSi amorphous high-entropy alloy film with a high corrosion-resistance in artificial sea water. *Appl. Surf. Sci.* **2021**, *542*, 148520–148529. [CrossRef]

65. Liu, H.; Gao, Q.; Hao, J.B.; Zhang, G.Z.; Hu, Y.; Yang, H.F. Microstructure and Corrosion Resistance of $AlCoCrFeNiSi_x$ High-Entropy Alloy Coating by Laser Cladding. *Rare Met. Mater. Eng.* **2022**, *51*, 2199–2208. (In Chinese)

66. Li, L.; Ye, H.; Liu, Y.; Zhang, K.; She, H.Y.; Qu, W.; Zhang, J.Y.; Yan, Z.L. Process Optimization and Corrosion Resistance of Laser Cladding AlCoCrFeNiCu High-entropy Alloy. *Surf. Technol.* **2022**, *51*, 388–396. (In Chinese)

67. Qiu, X.W.; Liu, C.G.; Zhang, Y.P. Microstructure and Property of $Al_2CoCrCuFeNi_x$Ti High Entropy Alloy Coatings Prepared by Laser Cladding. *LaserOptoelectron. Prog.* **2017**, *54*, 267–273. (In Chinese)

68. Archard, J.F.; Hirst, W. The Wear of Metals under Unlubricated Conditions. *Proc. R. Soc. London Ser. A Math. Phys. Sci.* **1956**, *236*, 397–410.

69. Guo, Y.X.; Liu, Q.B.; Zhou, F. Miscrostructure and wear rsistance of high-melting-point $AlCrFeMoNb_x$TiW high-entropy alloy coating coating by laser cladding. *Chin. J. Rare Met.* **2017**, *41*, 1327–1332. (In Chinese)

70. Liu, D.Z.; Zhao, J.; Li, Y.; Zhu, W.L.; Lin, L.X. Effects of Boron Content on Microstructure and Wear Properties of $FeCoCrNiB_x$ High-Entropy Alloy Coating by Laser Cladding. *Appl. Sci.* **2019**, *10*, 49. [CrossRef]

71. Wang, X.Y.; Huang, Y.B.; Liu, Q.; Xie, L.; Xu, Q.; Huang, J.X. Effect of molybdenum content on microstructure and wear resistance of laser-clad high-entropy alloy on carbon steel. *Electroplat. Finish.* **2020**, *39*, 1201–1208. (In Chinese)

72. Sha, C.H.; Zhou, Z.F.; Xie, Z.H.; Munroe, P. FeMnNiCoCr-based high entropy alloy coatings: Effect of nitrogen additions on microstructural development, mechanical properties and tribological performance. *Appl. Surf. Sci.* **2020**, *507*, 145101–145112. [CrossRef]

73. Xing, Q.; Feltrin, A.C.; Akhtar, F. High-temperature wear properties of CrFeHfMnTiTaV septenary complex concentrated alloy film produced by magnetron sputtering. *Wear* **2022**, *510–511*, 204497–204506. [CrossRef]

74. Tsai, M.H.; Wang, C.W.; Tsai, C.W.; Shen, W.J.; Yeh, J.W.; Gan, J.Y.; Wu, W.W. Thermal Stability and Performance of NbSiTaTiZr High-Entropy Alloy Barrier for Copper Metallization. *J. Electrochem. Soc.* **2011**, *158*, H1161–H1165. [CrossRef]

75. Jiang, C.; Li, R.; Wang, X.; Shang, H.; Zhang, Y.; Liaw, P.K. Diffusion Barrier Performance of AlCrTaTiZr/AlCrTaTiZr-N High-Entropy Alloy Films for Cu/Si Connect System. *Entropy* **2020**, *22*, 234. [CrossRef]

76. Zhang, C.; Huang, B.; Dai, P.Q. Effects of Chromium Content on Oxidation Behavior of FeCoCrxNiB High-entropy Alloy Coating. *China Surf. Eng.* **2016**, *29*, 32–38. (In Chinese)

77. Ma, M.Y.; Han, A.H.; Zhang, Z.J.; Lian, Y.; Zhao, C.; Zhang, J. The role of Si on microstructure and high-temperature oxidation of $CoCr_2FeNb_{0.5}Ni$ high-entropy alloy coating. *Corros. Sci.* **2021**, *185*, 109417–109426. [CrossRef]

78. Cui, W.Y.; Li, W.; Chen, W.T.; Liou, F. Laser Metal Deposition of an $AlCoCrFeNiTi_{0.5}$ High-Entropy Alloy Coating on a Ti6Al4V Substrate: Microstructure and Oxidation Behavior. *Crystals* **2020**, *10*, 638. [CrossRef]

79. Zhang, S.T.; Du, X.; Li, W.G.; Liu, Y.B.; Jiang, T.; Wu, X.F.; Zhong, N.; Zhao, Y.T. Preparation of FeCoCrNiMo High-entropy Alloy Coating and Its Oxidation Behavior. *Surf. Technol.* **2022**, *51*, 90–98, 110. (In Chinese)

80. Cai, Y.C.; Zhu, L.S.; Cui, Y.; Geng, K.P.; Marwana Manladan, S.; Luo, Z. High-temperature oxidation behavior of $FeCoCrNiAl_x$ high-entropy alloy coatings. *Mater. Res. Express* **2019**, *6*, 126552–126563. [CrossRef]

81. Zhang, F.Y.; Wang, L.Q.; Yan, S.; Yu, G.X.; Chen, J.W.; Yin, F.X. High temperature oxidation behavior of atmosphere plasma sprayed AlCoCrFeNi high-entropy alloy coatings. *Mater. Chem. Phys.* **2022**, *282*, 125939–125950. [CrossRef]

82. Luo, W.K.; Li, B.Y.; Zhao, Z.H.; Harumoto, T.; Nakamura, Y.; Shi, J. Study on magnetic properties and microstructure of $Fe_{0.18}Co_{0.36}Ni_{0.21}Al_{0.10}Cr_{0.15}$ high entropy alloy thin films. *J. Alloys Compd.* **2023**, *938*, 168533–168540. [CrossRef]
83. Huang, H.; Liaw, P.K.; Zhang, Y. Structure design and property of multiple-basis-element (MBE) alloys flexible films. *Nano Res.* **2021**, *15*, 4837–4844. [CrossRef]
84. Huang, H.; Zhang, Y. High-entropy alloy and metallic glass flexible materials. *Chin. J. Eng.* **2021**, *43*, 119–128. (In Chinese)